

## Well parameters of two-dimensional electron gas in $\text{Al}_{0.88}\text{In}_{0.12}\text{N}/\text{AlN}/\text{GaN}/\text{AlN}$ heterostructures grown by MOCVD

P. Taslı\*<sup>1</sup>, S. B. Lisesivdin<sup>2</sup>, A. Yildiz<sup>3,4</sup>, M. Kasap<sup>1</sup>, E. Arslan<sup>2</sup>, S. Özcelik<sup>1</sup>, and E. Ozbay<sup>2,5</sup>

<sup>1</sup> Dept. of Physics, Faculty of Science and Arts, University of Gazi, Teknikokullar, 06500 Ankara, Turkey

<sup>2</sup> Nanotechnology Research Center, Bilkent University, Bilkent, 06800 Ankara, Turkey

<sup>3</sup> Dept. of Physics, Faculty of Science and Arts, Ahi Evran University, Aşıkpaşa Kampüsü, 40040 Kırşehir, Turkey

<sup>4</sup> Dept. of Engineering Physics, Faculty of Engineering, Ankara University, 06100 Besevler, Ankara, Turkey

<sup>5</sup> Dept. of Physics, Bilkent University, Bilkent, 06800 Ankara, Turkey and Dept. of Electrical and Electronics Engineering, Bilkent University, Bilkent, 06800 Ankara, Turkey

Received 1 September 2009, accepted 19 November 2009

Published online 1 December 2009

**Key words** 2DEG, 2DHG, AlInN/GaN, QMSA.

**PACS** 73.20.-r, 73.21.Fg, 73.40c, 73.50.Dn, 73.61.Ey

Resistivity and Hall effect measurements were carried out as a function of magnetic field (0–1.5 T) and temperature (30–300 K) for  $\text{Al}_{0.88}\text{In}_{0.12}\text{N}/\text{AlN}/\text{GaN}/\text{AlN}$  heterostructures grown by Metal Organic Chemical Vapor Deposition (MOCVD). Magnetic field dependent Hall data were analyzed by using the quantitative mobility spectrum analysis (QMSA). A two-dimensional electron gas (2DEG) channel located at the  $\text{Al}_{0.88}\text{In}_{0.12}\text{N}/\text{GaN}$  interface with an AlN interlayer and a two-dimensional hole gas (2DHG) channel located at the GaN/AlN interface were determined for  $\text{Al}_{0.88}\text{In}_{0.12}\text{N}/\text{AlN}/\text{GaN}/\text{AlN}$  heterostructures. The interface parameters, such as quantum well width, the deformation potential constant and correlation length as well as the dominant scattering mechanisms for the  $\text{Al}_{0.88}\text{In}_{0.12}\text{N}/\text{GaN}$  interface with an AlN interlayer were determined from scattering analyses based on the exact 2DEG carrier density and mobility obtained with QMSA.

© 2010 WILEY-VCH Verlag GmbH & Co. KGaA, Weinheim

### 1 Introduction

The development of advanced high electron mobility transistors (HEMTs) is continuously growing and  $\text{Al}_x\text{Ga}_{1-x}\text{N}/\text{GaN}$  based HEMTs have attracted enormous attention for high-power and high-temperature applications at microwave and millimeter-wave frequencies [1]. In wurtzite GaN-based heterostructures with [0001] orientation, strong polarization fields are formed. These fields are known as the spontaneous (or pyroelectric) polarization field and the strain induced piezoelectric polarization field [2], in which these fields largely influence the band structures and electron densities of these heterostructures. Traditional  $\text{Al}_x\text{Ga}_{1-x}\text{N}/\text{GaN}$  HEMTs are generally designed by depositing a layer of  $\text{Al}_x\text{Ga}_{1-x}\text{N}$  on a thick GaN epilayer on a semi-insulating substrate. However, recent improvements have been made in the growth and design of this material system by use of AlN layers. Firstly, the insertion of an AlN buffer layer between GaN buffer layer and a sapphire substrate effectively reduces dislocation scattering and results in an increase in both mobility and carrier density [3,4]. Secondly, the insertion of a thin AlN interlayer at the  $\text{Al}_x\text{Ga}_{1-x}\text{N}/\text{GaN}$  interface also reduces the effect of alloy scattering and again results in an increase in mobility and carrier density [5].

Recently,  $\text{Al}_x\text{In}_{1-x}\text{N}/\text{AlN}/\text{GaN}$  heterostructures have been proposed as active layers for heterostructures in turn essentially predicting higher carrier densities than that of  $\text{Al}_x\text{Ga}_{1-x}\text{N}/\text{AlN}/\text{GaN}$  heterostructures [6]. The advantage of using an  $\text{Al}_x\text{In}_{1-x}\text{N}$  barrier is to adjust the composition of the alloys in order to obtain lattice

\* Corresponding author: e-mail: pttasli@gmail.com

matched heterostructures [7]. The ability of  $\text{Al}_x\text{In}_{1-x}\text{N}$  with  $\sim 18\%$  In content ( $x \sim 0.82$ ) that is to be grown lattice matched with respect to GaN is expected to allow for the growth of good material with lower defect density compared to traditional  $\text{Al}_x\text{Ga}_{1-x}\text{N}/\text{AlN}/\text{GaN}$  heterostructures [8]. Therefore, investigations on  $\text{Al}_x\text{In}_{1-x}\text{N}$  and  $\text{Al}_x\text{In}_{1-x}\text{N}/\text{AlN}/\text{GaN}$  heterostructures in the literature are increasing to some extent. On the other hand,  $\text{Al}_x\text{Ga}_{1-x}\text{N}/\text{GaN}/\text{AlN}$  heterostructures (with an AlN buffer layer) are reported to have both two-dimensional electron gas (2DEG) and two-dimensional hole gas (2DHG) at the  $\text{Al}_x\text{Ga}_{1-x}\text{N}/\text{GaN}$  interface and GaN/AlN interfaces, respectively [3,4,9]. Just as in  $\text{Al}_x\text{Ga}_{1-x}\text{N}/\text{GaN}/\text{AlN}$  heterostructures, the valence band edge can cross the Fermi level at the GaN/AlN interface in  $\text{Al}_x\text{In}_{1-x}\text{N}/\text{AlN}/\text{GaN}/\text{AlN}$  heterostructures. Thus, in  $\text{Al}_{0.88}\text{In}_{0.12}\text{N}/\text{AlN}/\text{GaN}/\text{AlN}$  heterostructures, 2DEG carriers will be formed at the  $\text{Al}_{0.88}\text{In}_{0.12}\text{N}/\text{GaN}$  interface with an AlN interlayer and 2DHG carriers can also be formed at the GaN/AlN interface.

Generally, the investigations of the transport properties of heterostructures are studied by using single field Hall effect measurements. The single field Hall effect measurements can give only the weighted average carrier density as well as the mobility of all the carriers in the sample. Therefore, the obtained information about transport properties heterostructures may be misleading since multi-carrier conduction is expected, such as in  $\text{Al}_x\text{Ga}_{1-x}\text{N}/\text{AlN}/\text{GaN}/\text{AlN}$  and  $\text{Al}_x\text{In}_{1-x}\text{N}/\text{AlN}/\text{GaN}/\text{AlN}$  [4,10,11]. Quantitative mobility spectrum analysis (QMSA) in conjunction with variable magnetic field Hall measurements provides the extraction of the individual carrier mobilities and densities in many semiconductor structures including bulk structures, thin films and multi layer devices [12-15].

The main purpose of the present study is to determine the dominant scattering mechanisms and interface related parameters, such as quantum well width ( $Z$ ), deformation potential constant ( $\Xi$ ) and correlation length of the roughness ( $\Lambda$ ) of  $\text{Al}_{0.88}\text{In}_{0.12}\text{N}/\text{AlN}/\text{GaN}/\text{AlN}$  heterostructures in the  $\text{Al}_{0.88}\text{In}_{0.12}\text{N}/\text{GaN}$  interface with an AlN interlayer. To perform this, the 2DEG parameters (carrier density and mobility) were extracted from the variable field Hall data by using QMSA. The interface parameters were then obtained from the scattering analysis based on the extracted 2DEG carrier density and mobility in  $\text{Al}_{0.88}\text{In}_{0.12}\text{N}/\text{AlN}/\text{GaN}/\text{AlN}$  heterostructures.

## 2 Experimental

The  $\text{Al}_{0.88}\text{In}_{0.12}\text{N}/\text{AlN}/\text{GaN}/\text{AlN}$  heterostructures on c-plane (0001)  $\text{Al}_2\text{O}_3$  substrate were grown in a low-pressure MOCVD reactor. Prior to epitaxial growth,  $\text{Al}_2\text{O}_3$  substrate was annealed at  $1100^\circ\text{C}$  for 10 min in order to remove surface contamination. The growth was initiated with a 10 nm thick low-temperature ( $840^\circ\text{C}$ ) AlN nucleation layer. Then, a 420 nm high-temperature (HT) AlN buffer layer was grown at a temperature of  $1150^\circ\text{C}$ . A  $1.3\ \mu\text{m}$  thick undoped GaN buffer layer (BL) was then grown at  $1070^\circ\text{C}$  and a reactor pressure of 200 mbar. After the GaN BL, a nearly 2.4 nm thick HT-AlN layer was grown at  $1085^\circ\text{C}$  with a pressure of 50 mbar. Then, an HT-AlN layer was followed by an 11.6 nm thick AlInN ternary layer. This layer was grown at  $800^\circ\text{C}$  and a pressure of 50 mbar. Finally, a 2.4 nm thick GaN cap layer growth was carried out at a temperature of  $1085^\circ\text{C}$  and a pressure of 50 mbar. All the layers are nominally undoped. Indium mole fractions of the barrier layers were determined by high-resolution x-ray diffraction (XRD) measurements. The details of the samples are shown in figure 1.

For the resistivity and Hall effect measurements by the van der Pauw method, square shaped ( $5 \times 5\ \text{mm}^2$ ) samples were prepared with four evaporated triangular Ti/Al/Ni/Au ohmic contacts in the corners. With indium soldering, the electrical contacts were made and their ohmic behavior was confirmed by the current-voltage (I-V) characteristics. The measurements were performed at 14 temperature steps in the temperature interval of 30-300 K by using a Lake Shore Hall effect measurement system (HMS). At each temperature step, the Hall coefficient (with max. 5 % error) and resistivity (with max. 0.2 % in the studied range) were measured for both current directions, both magnetic field polarizations, and all the possible contact configurations at a 20 magnetic field step between 0 and 1.5 T. The magnetic field dependent data were analyzed by using the improved QMSA (i-QMSA) [16] technique (herein referred to as simply "QMSA").

## 3 Results and discussion

The resistivity and Hall measurements of  $\text{Al}_{0.88}\text{In}_{0.12}\text{N}/\text{AlN}/\text{GaN}/\text{AlN}$  heterostructures as a function of the magnetic field (0-1.5 T) were carried out at 14 temperatures steps in the temperature interval of 30-300 K. The

quantum effects in the magnetic field dependent resistivity were not observed at any temperature steps. To obtain conductivity tensors ( $\sigma_{xx}$ ,  $\sigma_{xy}$ ) and then the multi carrier spectra, the QMSA technique was applied to the magnetic field dependent resistivity and Hall data at each temperature step. For the demonstration, the derived experimental conductivity tensors and the QMSA fit results are given in figure 2a for 50 K and 269 K. The near perfect fit to the data is a good indication of the validity of the mobility spectrums obtained from QMSA.

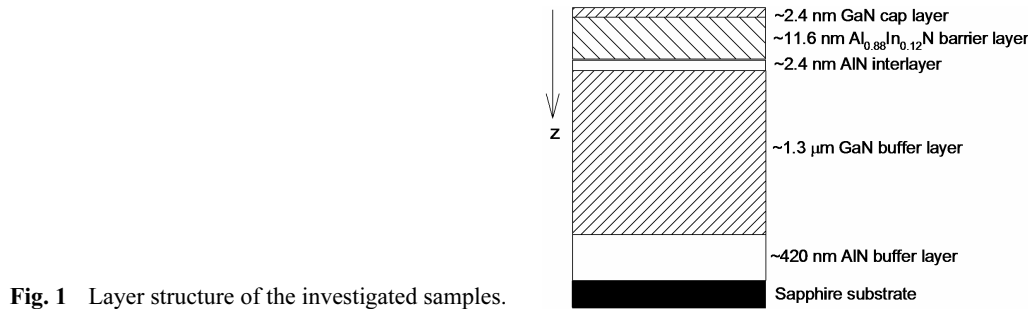


Fig. 1 Layer structure of the investigated samples.

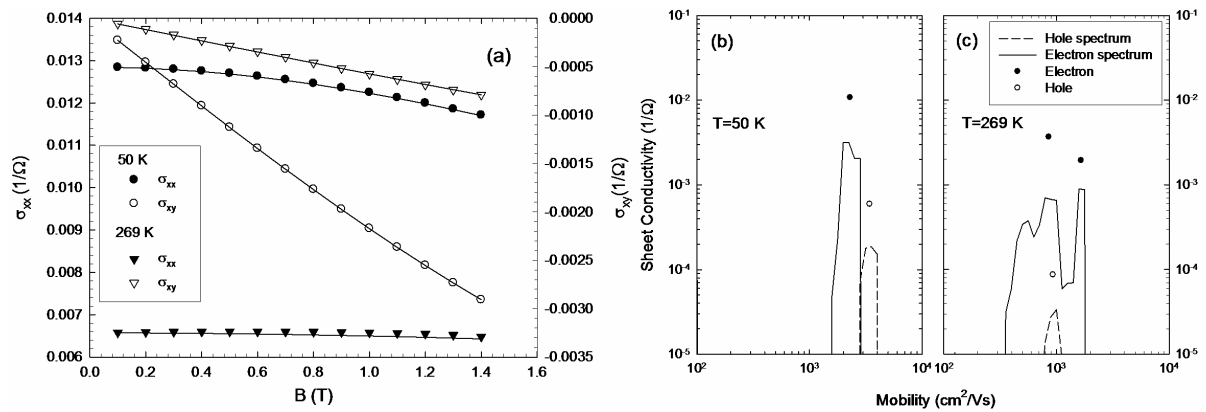


Fig. 2 (a) Conductivity tensors versus magnetic field at 50 and 269 K. The symbols and lines represent the experiment and QMSA fits, respectively. Mobility spectra obtained with using QMSA at (b) 50 K and (c) 269 K. Calculated carriers are shown with symbols.

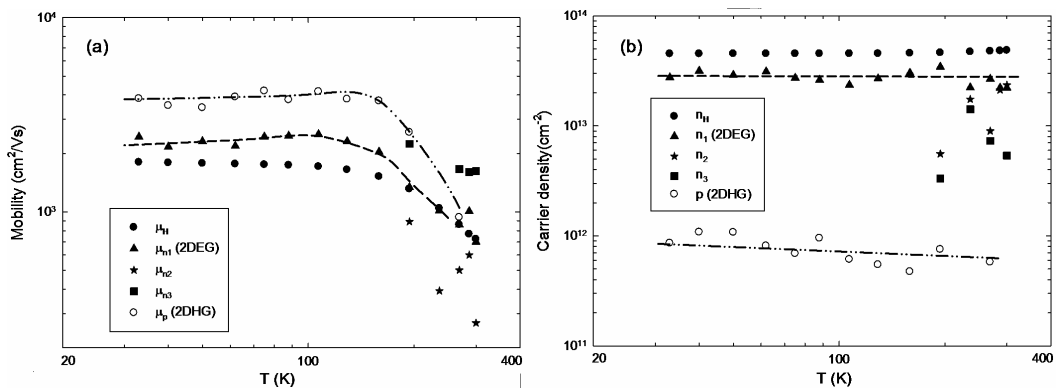


Fig. 3 (a) Mobility and (b) carrier density versus temperature. The closed circles represent the measured mobility and carrier density taken at 0.5 Tesla. The triangles represent the extracted 2DEG mobility and carrier density. The open circles represent the extracted 2DHG mobility and carrier density. The stars and squares represent the bulk carriers. The lines are guide for the eyes.

Figure 2b and c represents the mobility spectra obtained from QMSA at 50 K and 269 K, respectively. With QMSA, one electron peak and one hole are observed at each temperature in the studied temperature range while up to three electron peaks are observed at high temperatures. Carriers which correspond to related peaks

are shown as filled and empty symbols for electrons and holes, respectively. Figure 3a and b shows all QMSA results as a function of temperature for the mobility and integrated density for  $\text{Al}_{0.88}\text{In}_{0.12}\text{N}/\text{AlN}/\text{GaN}/\text{AlN}$  heterostructures, respectively. In the figure, the mobilities and carrier densities measured at 0.5 T are also given for a comparison. To clearly extract carriers in a sample, dimensionless product of the lowest mobility and highest field must be greater than unity ( $\mu_{\min} B_{\max} \geq 1$ ). For the QMSA studies,  $\mu_{\min} B_{\max} \approx 0.5$  condition can be accepted as a limit [16]. For the present study, this condition seems to be barely satisfied, in which the results scatter in the QMSA data. However, we successfully showed extracted 2DEG and two-dimensional hole gas (2DHG) carriers with low mobilities in  $\text{AlGaIn}/\text{GaIn}/\text{AlIn}$  heterostructures in a previous study.<sup>9</sup> From Fig. 3 (a) and (b), it can be seen that one electron (denoted with triangles) and one hole carrier (denoted with circles), which are obtained from QMSA, are contributing to charge transport throughout the entire studied temperature range. At high temperatures, the mobilities of both carriers decrease with increasing temperature while they are independent of temperature at low temperatures. On the other hand, both carrier densities are also nearly independent of temperature in the studied temperature range. These behaviors of mobilities and carrier densities extracted from QMSA are typical of 2DEG and 2DHG behaviors.

**Table 1** Material parameters i.e. elastic constants, piezoelectric constants, spontaneous polarization and the lattice parameters of InN, AlN and GaN.

Parameter	InN	GaN	AlN
$a$ (nm)	0.3540	0.3189	0.3112
$e_{31}$ (C/m <sup>2</sup> )	-0.57	-0.35	-0.50
$e_{33}$ (C/m <sup>2</sup> )	0.97	1.27	1.79
$C_{13}$ (GPa)	92	106	108
$C_{33}$ (GPa)	224	398	373
$P_{SP}$ (C/m <sup>2</sup> )	-0.042	-0.034	-0.090

One might expect extracted hole carriers may be classified as “ghost holes” which is reported elsewhere [13]. If there is no possibility to occur positive charge carriers in according to band structure, polarization mechanisms, doping scheme and growth conditions, the hole peaks obtained from QMSA can then be generally accepted as ghost holes. However, our structures have a GaN/AlN interface where holes can be populated since the valence band edge of  $\text{Al}_{0.88}\text{In}_{0.12}\text{N}/\text{AlN}/\text{GaIn}/\text{AlIn}$  heterostructures crosses the Fermi level near the GaN/AlN interface. To confirm this, we have simulated the room temperature band diagram of the studied  $\text{Al}_{0.88}\text{In}_{0.12}\text{N}/\text{AlN}/\text{GaIn}/\text{AlIn}$  heterostructures by using *nextnano3* [17]. In simulations, Schrödinger’s and Poisson’s equations are both solved self-consistently in order to obtain the carrier distribution, wave functions, and related eigenenergies. The material parameters i.e. elastic constants, piezoelectric constants, spontaneous polarization and the lattice parameters of InN, AlN and GaN, are listed in table 1 [18-21]. For the  $\text{Al}_x\text{In}_{1-x}\text{N}$  layers, lattice parameters, elastic constants and piezoelectric constants are calculated with Vegard’s law using the parameters of InN and AlN. For the spontaneous polarization at  $\text{Al}_x\text{In}_{1-x}\text{N}$  layer, following bowing formula is used [18].

$$P_{SP}^{\text{Al}_x\text{In}_{1-x}\text{N}} = xP_{SP}^{\text{AlN}} + (1-x)P_{SP}^{\text{InN}} + 0.070x(1-x). \quad (1)$$

As shown in figure 4a and b, it is clear that the simulations indicate the formation of the 2DHG carriers at the GaN/AlN interface and the formation of 2DEG carriers at the  $\text{Al}_{0.88}\text{In}_{0.12}\text{N}/\text{GaIn}$  interface with an AlN interlayer. Therefore, from figure 3b, it is clearly understood that polarization induced 2DEG and 2DHG carriers, and the thermally activated bulk-related carriers are presented in  $\text{Al}_{0.88}\text{In}_{0.12}\text{N}/\text{AlN}/\text{GaIn}/\text{AlIn}$  heterostructures. These thermally activated carriers are attributed to the donor levels of unintentionally doped bulk GaN [22]. The 2DEG carriers are due to the high spontaneous polarizations at the  $\text{Al}_{0.88}\text{In}_{0.12}\text{N}/\text{GaIn}$  interface with an AlN interlayer of  $\text{Al}_{0.88}\text{In}_{0.12}\text{N}/\text{AlN}/\text{GaIn}/\text{AlIn}$  heterostructures. Although the temperature dependence of sheet carrier density and the mobility of both channels are similar, the mobility values of 2DHG carriers are slightly higher than that of 2DEG carriers, while the density of 2DHG carriers are lower than 2DEG carriers. Therefore, the contribution of the 2DEG channel to total conductivity is higher than that of the 2DHG channel. On the other hand, our simulations show that 2DEG only has one occupied subband and the second subband lies just above the Fermi level in the investigated samples as shown in figure 4a. However, the second subband occupancy can be expected for structures with similar Indium mole fractions and barrier thicknesses.

**Fig. 4** Simulated band diagrams of (a) 2DEG well and (b) 2DHG well for  $\text{Al}_{0.88}\text{In}_{0.12}\text{N}/\text{AlN}/\text{GaN}/\text{AlN}$  heterostructures. Conduction and valence bands are shown with red and blue lines, respectively. Insert: Details of the quantum well. Wavefunctions of the first two subbands are shown with green dash-dot lines. (Online color at [www.crt-journal.org](http://www.crt-journal.org))

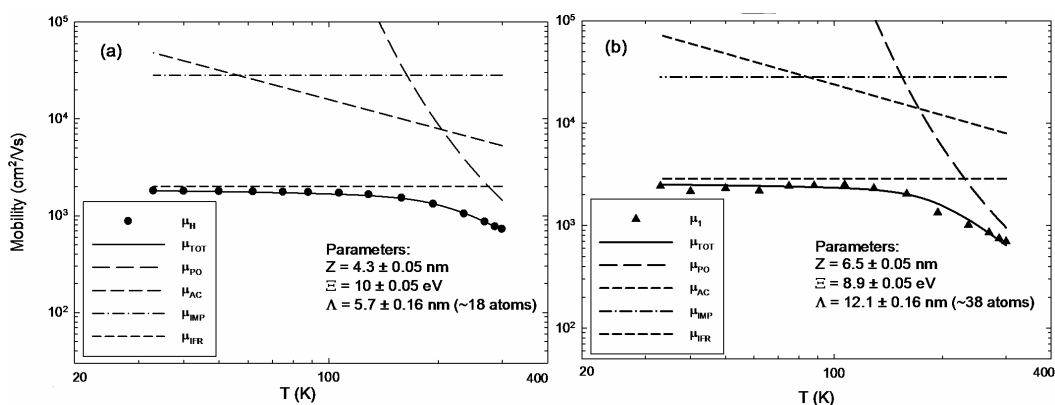
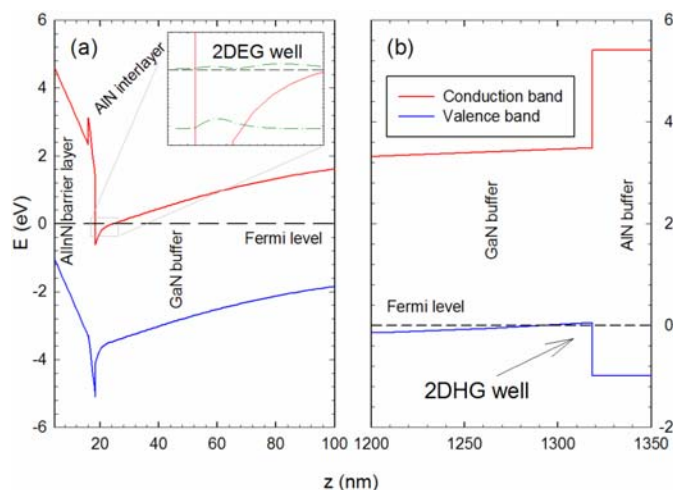


**Fig. 5** Scattering analysis of (a) measured mobility (using the Hall data) and (b) extracted mobility (using the QMSA data) versus temperature.

To deeply understand the transport properties of the single subband 2DEG channel located near the  $\text{Al}_{0.88}\text{In}_{0.12}\text{N}/\text{GaN}$  interface, scattering analyses were carried out by using the data extracted with QMSA for the 2DEG channel as well as the measured single field Hall data for comparison purposes. The scattering mechanisms of the two-dimensional carriers in III-V heterojunctions are well described [22,23]. In our analyses, polar optical phonon scattering (PO), acoustic phonon scattering (AC) (which includes deformation potential scattering and piezoelectric scattering), background impurity scattering (IMP), and interface roughness scattering (IFR) were used. Because of the AlN interlayer, alloy scattering was not included in our analyses. The expressions of scattering mechanisms and the parameters used in the calculation are given elsewhere [22]. In the calculations, quantum well width ( $Z$ ), deformation potential constant ( $\Xi$ ) and correlation length of the roughness ( $\Lambda$ ) were used as adjustable parameters. The results are shown in figure 5a and b. As can be seen in the figure, a good fit in both cases (the scattering analysis based on the single field Hall data and the scattering analyses based on the extracted data) were obtained by using the fitting parameters as given in the figure. The scattering analyses based on the extracted data show that the low temperature ( $T < 200$  K) mobility is limited only by the interface roughness scattering mechanism, while at the high temperature ( $T > 200$  K) the optical phonon scattering is the dominant scattering mechanism. Also, the interface roughness scattering mechanism has a strong influence on the mobility even at high temperatures. The effect of acoustic phonon scattering is negligible. In the entire studied temperature range, the strong effect of interface roughness scattering mechanism results in a low mobility material. The strong effect of interface roughness scattering can be attributed to the thick AlN interlayer. With a thick AlN interlayer, interface roughness will be increased due to increased partial strain relaxation probability. This result is in good agreement with the studies that report similar findings for  $\text{AlInN}/\text{AlN}/\text{GaN}$  [6,24] and  $\text{AlGaIn}/\text{AlN}/\text{GaN}$  heterostructures having different thicknesses of AlN interlayers [25]. These studies reported low mobilities with the use of thick AlN interlayers. In a recent

study, effects of AlN thicknesses on transport properties are studied in details, and 1 nm AlN interlayer thickness is suggested as an optimal thickness [26].

There are significant differences between the fitting parameters obtained from the scattering analysis by using the data extracted with QMSA and the single field Hall data. The scattering analyses, which use the extracted data, predict a smaller deformation potential value and a higher quantum well width and the correlation length values than those obtained from the single field scattering analyses. We suggest that the parameters obtained from the analyses based only on the 2DEG mobility and density for the  $\text{Al}_{0.88}\text{In}_{0.12}\text{N}/\text{GaN}$  interface with an AlN interlayer are more accurate, since these analyses do not include the effect of the 2DHG channel located near the GaN/AlN interface and the bulk carriers. Therefore, the values of the quantum well width of  $Z = 6.5 \pm 0.05$  nm, the deformation potential constant of  $\Xi = 8.9 \pm 0.05$  eV and the correlation length of the roughness of  $\Lambda = 12.1 \pm 0.16$  nm represent the real merit of the  $\text{Al}_{0.88}\text{In}_{0.12}\text{N}/\text{GaN}$  interface when compared with the Fermi wavelength well-width approximation [27] and the deformation potential calculation [28]. The well width is also an important parameter, which affects the polar optic phonon scattering and background impurity scattering. With QMSA usage, more accurate scattering analyses can be performed. In the studied samples, the interface roughness scattering mechanism has a strong influence, even at higher temperatures than those seen in AlGaIn/GaN heterostructures [22]. This leads to a higher correlation length, since the mobility limited by this mechanism is inversely proportional to the square of the correlation length ( $\mu \propto 1/\Lambda^2$ ). With a thinner AlN interlayer and growths that lead to smooth interfaces, the influence of interface roughness scattering can be decreased, and thereby the mobility may be increased up to the background impurity scattering limit.

## 4 Conclusions

Variable temperature (30-300 K) and magnetic field (0-1.5 T) Hall Effect measurements were carried out for undoped  $\text{Al}_{0.88}\text{In}_{0.12}\text{N}/\text{AlN}/\text{GaN}/\text{AlN}$  heterostructures grown by MOCVD. The QMSA results show that a single subband 2DEG channel located at the  $\text{Al}_{0.88}\text{In}_{0.12}\text{N}/\text{GaN}$  interface with an AlN interlayer and a 2DHG channel located at the GaN/AlN interface contribute to the total conductivity in  $\text{Al}_{0.88}\text{In}_{0.12}\text{N}/\text{AlN}/\text{GaN}/\text{AlN}$  heterostructures. The contribution of the 2DEG channel to the total conductivity is higher than that of the 2DHG channel. The values of the quantum well width of  $Z = 6.5 \pm 0.05$  nm, the deformation potential constant of  $\Xi = 8.9 \pm 0.05$  eV, and the correlation length of the roughness at the interface as  $\Lambda = 12.1 \pm 0.16$  nm are all obtained from the scattering analyses based on the 2DEG data extracted by using QMSA. It was also found that the interface roughness scattering was the only dominant scattering mechanism at low temperatures while both the optical phonon and the interface roughness scattering mechanisms dominated the mobility at high temperatures. The reason for the strong influence of interface roughness scattering is attributed to the use of a thick (~2.4 nm) AlN interlayer. The strong effect of the interface roughness scattering brings about low mobility  $\text{Al}_{0.88}\text{In}_{0.12}\text{N}/\text{AlN}/\text{GaN}/\text{AlN}$  heterostructures, which can be improved with thinner AlN interlayer use as well as with growths that lead to smooth interfaces.

**Acknowledgements** This work is supported by the State of Planning Organization of Turkey under grant no. 2001K120590 and European Union under the projects EU-PHOME, and EU-ECONAM, and TUBITAK under Project Nos. 106E198, 107A004, and 107A012. One of the authors (E.O.) also acknowledges partial support from the Turkish Academy of Sciences.

## References

- [1] M. A. Khan, Q. Chen, M. S. Shur, B. T. Dermott, J. A. Higgins, J. Burm, W. Schaff, and L. F. Eastman, *Electron Lett.* **32**, 357 (1996).
- [2] O. Ambacher, B. Foutz, J. Smart, J. R. Shealy, N. G. Weimann, K. Chu, M. Murphy, A. J. Sierakowski, W. J. Schaff, L. F. Eastman, R. Dimitrov, A. Mitchell, and M. Stutzmann, *J. Appl. Phys.* **87**, 334 (2000).
- [3] X. Hu, J. Deng, N. Pala, R. Gaska, M. S. Shur, C. Q. Chen, J. Yang, G. Simin, M. A. Khan, J. C. Rojo, and L. J. Schowalter, *Appl. Phys. Lett.* **82**, 1299 (2003).
- [4] Z. Y. Fan, J. Li, M. L. Nakarmi, J. Y. Lin, and H. X. Jiang, *Appl. Phys. Lett.* **88**, 073513 (2006).
- [5] P. Smorchkova, L. Chen, T. Mates, L. Shen, S. Heikman, B. Moran, S. Keller, S. P. DenBaars, J. S. Speck, and U. K. Mishra, *J. Appl. Phys.* **90**, 5196 (2001).

- [6] J. Xie, X. Ni, M. Wu, J. H. Leach, Ü. Özgür, and H. Morkoç, *Appl. Phys. Lett.* **91**, 132116 (2007).
- [7] R. Tulek, A. Ilgaz, S. Gokden, A. Teke, M. K. Ozturk, M. Kasap, S. Ozcelik, E. Arslan, and E. Ozbay, *J. Appl. Phys.* **105**, 013707 (2009).
- [8] A. Dadgar, F. Schulze, J. Blasing, A. Diez, and A. Krost, *Appl. Phys. Lett.* **85**, 5400 (2004).
- [9] S. Acar, S. B. Lisesivdin, M. Kasap, S. Ozcelik, and E. Ozbay, *Thin Solid Films* **516**, 2041 (2008).
- [10] M. Gonschorek, J. F. Carlin, E. Feltin, M. A. Py, N. Grandjean, V. Darakchieva, B. Monemar, M. Lorenz, and G. Ramm, *J. Appl. Phys.* **103**, 093714 (2008).
- [11] A. Dadgar, M. Neuberger, F. Schulze, J. Blasing, A. Krtschil, I. Daumiller, M. Kunze, K. M. Gunther, H. Witte, A. Diez, E. Kohn, and A. Krost, *Phys. Status Solidi A* **202**, 832 (2005).
- [12] J. R. Meyer, C. A. Hoffman, J. Antoszewski, and L. Faraone, *J. Appl. Phys.* **81**, 709 (1997).
- [13] N. Biyikli, J. Xie, Y. T. Moon, F. Yun, C. G. Stefanita, S. Bandyopadhyay, H. Morkoç, I. Vurgaftman, and J. R. Meyer, *Appl. Phys. Lett.* **88**, 142106 (2006).
- [14] J. Antoszewski, D. J. Seymour, L. Faraone, J. R. Meyer, and C. A. Hoffman, *J. Electron. Mater.* **24**, 1255 (1995).
- [15] B. C. Dodrill, J. R. Lindemuth, B. J. Kelley, G. Du, and J. R. Meyer, *Compound Semicond.* **7**, 58 (2001).
- [16] I. Vurgaftman, J. R. Meyer, C. A. Hoffman, D. Redfern, J. Antoszewski, L. Faraone, and J. R. Lindemuth, *J. Appl. Phys.* **84**, 4966 (1998).
- [17] S. Birner, S. Hackenbuchner, M. Sabathil, G. Zandler, J. A. Majewski, T. Andlauer, T. Zibold, R. Morschl, A. Trellakis, and P. Vogl, *Acta Phys. Pol. A* **110**, 111 (2006).
- [18] I. Vurgaftman and J. R. Meyer, *J. Appl. Phys.* **96**, 3675 (2003).
- [19] I. Vurgaftman, J. R. Meyer, and L. R. Ram-Mohan, *J. Appl. Phys.* **89**, 5815 (2001).
- [20] O. Ambacher, J. Majewski, C. Miskys, A. Link, M. Hermann, M. Eickhoff, M. Stutzmann, F. Bernardini, V. Fiorentini, V. Tilak, B. Schaff, and L. F. Eastman, *J. Phys.: Condens. Matter* **14**, 3399 (2002).
- [21] H. Morkoç, *Nitride Semiconductors and Devices*, (Springer-Verlag, Berlin Heidelberg, 1999).
- [22] S. B. Lisesivdin, S. Acar, M. Kasap, S. Ozcelik, S. Gokden, and E. Ozbay, *Semicond. Sci. Technol.* **22**, 543 (2007).
- [23] D. Zanato, S. Gokden, N. Balkan, B. K. Ridley, and W. J. Schaff, *Semicond. Sci. Technol.* **19**, 427 (2004).
- [24] M. Gonschorek, J.-F. Carlin, E. Feltin, M. A. Py, and N. Grandjean, *Appl. Phys. Lett.* **89**, 062106 (2006).
- [25] Y. Cao and D. Jena, *Appl. Phys. Lett.* **90**, 182112 (2007).
- [26] A. Teke, S. Gökden, R. Tulek, J. H. Leach, Q. Fan, J. Xie, Ü. Özgür, H. Morkoç, S. B. Lisesivdin, and E. Özbay, *New J. Phys.* **11**, 063031 (2009).
- [27] S. Gokden, *Physica E* **23**, 114 (2004).
- [28] L. Hsu and W. Walukiewicz, *Phys. Rev. B* **56**, 1520 (1997).